Precision radio-frequency measurements of the high-L Rydberg states of lithium

N. E. Rothery, C. H. Storry, and E. A. Hessels
York University, 4700 Keele Street, Toronto, Ontario, Canada
(Received 20 July 1994; revised manuscript received 10 November 1994)

The $n=10$ G-to-H and H-to-I intervals in lithium atoms have been measured to an accuracy of approximately 10 parts per million. The experiment utilizes a beam of Rydberg lithium atoms produced via a resonant charge-exchange technique and the measurements were performed using precision rf spectroscopy coupled with a laser-excitation and Stark-ionization detection technique. The results are compared with recently published polarization-model calculations of the fine structure of lithium and with a hydrogenic model of its spin structure. With the availability of more precise theory, further tests of relativistic and QED effects in this simple three-electron atom will be possible. Such tests could shed light on the discrepancies found between similar high-precision measurement and theory in helium. The measured values are 338.4778(33), 341.4027(35), 108.4819(51), and 110.1566(54) MHz for the intervals $10G_{9/2}$ to $10H_{11/2}$, $10G_{7/2}$ to $10H_{9/2}$, $10H_{11/2}$ to $10I_{13/2}$, and $10H_{9/2}$ to $10I_{11/2}$, respectively.

PACS number(s): 32.30.Bv, 34.60.+z

INTRODUCTION

In the present work, precise measurements of the lithium atom's $10G$-to-$10H$ and $10H$-to-$10I$ intervals are made. Over the past decade great advances have been made in our understanding of both the theory and experiment of the high-L fine structure of helium Rydberg states. It is hoped that the present work will lead to the extension of this precise understanding of Rydberg states up to the three-electron lithium atom. The early precise calculations in helium were performed by Drachman using a polarization model in 1982 [1]. Precise measurements of this structure followed in 1984 by Palfrey and Lundeen [2]. A variety of relativistic, radiative, and retardation effects was then tested by a series of developments made in both theory [3] and experiment [4] with a notable advance in theory made by Drake's variational calculations. Comparison of the most recent calculations by Drake [5] and the most recent precision measurements [6] reveals discrepancies much larger than the uncertainties in either.

Rydberg states of lithium consist of a two-electron (heliumlike) core and a distant Rydberg electron. These states are more complicated than the Rydberg states of helium, where both the Rydberg electron and core electron are in nearly hydrogenic orbits. Despite this complication, precise calculations are beginning to become available for these states. Bhatia and Drachman have carried out [7] polarization-model calculations by calculating the polarizabilities of Li using Hylleraas-style wave functions. Also, McKenzie and Drake have recently used variational methods to calculate [8] the ground-state energies of neutral lithium, and it appears that their method will eventually be expanded to include excited states as well. Thus the development of the theory of lithium appears to be paralleling the early theoretical developments in helium. By comparing sufficiently precise theory and measurements of the fine structure of lithium, tests of the relativistic and radiative effects of this simple three-electron atom will be possible. These tests are of increased interest because of the discrepancies found in the similar states of helium.

Previous measurements of the Rydberg states of lithium have been restricted to nD-to-nF and nD-to-nG ($n=7-11$) intervals, which were measured by Cooke, *et al.* [9] to an accuracy of 300–5000 kHz. Polarization-model predictions of Drachman and Bhatia [10] are for higher-L states and currently made to an accuracy of 100 kHz for the $10G$-to-H interval and 1 kHz for the $10H$-to-I interval. The measurements reported here for the $10G$-to-H and $10H$-to-I intervals in lithium are at accuracies of 3 and 5 kHz, respectively.

EXPERIMENT

A schematic of the apparatus used for the present measurement is shown in Fig. 1. Intense beams of Rydberg lithium or helium atoms were produced via a resonant charge-exchange technique. A Colutron ion source (with a velocity spread of less than 0.1%) was employed to create and accelerate a beam of either helium or lithium ions to a speed of $\beta=0.001\,03$ (at 1 in Fig. 1). Acceleration potentials of 3.5 and 2.0 kV were required to achieve beams at this β for $^7Li^+$ and $^4He^+$, respectively. A crossed electric- and magnetic-field velocity filter was

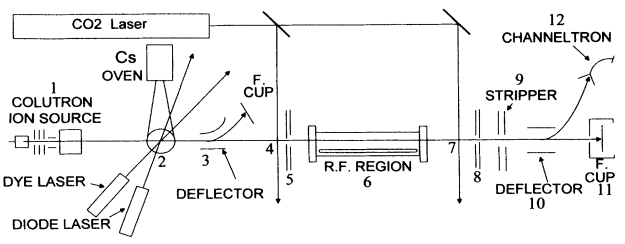

FIG. 1. Schematic of the experimental setup. The details of the setup are discussed in the text.

used to select out the particular ion of interest. Modification of the Colutron oven and feed system to allow for larger lithium charges was required in order to run intense, stable beams of lithium for many hours.

The ions created in the source pass through a target of excited Cs atoms (at 2 in Fig. 1) where the resonant charge exchange takes place. A thermal beam of cesium provides densities in the target region of approximately 10^{12} atoms/cm^3. The cesium is excited up to Rydberg states using a two-step laser excitation. For the first step a Northern Telecom LT50A-03U diode laser provides approximately 25 mW at 852 nm to excite the Cs from the ground $6S_{1/2}$ state to the $6P_{3/2}$ state. The diode laser primarily excites the cycling transition from $F=4$ $6S_{1/2}$ to $F=5$ $6P_{3/2}$. The second transition is made by a Coherent 599 dye laser pumped by an argon laser. The dye laser provides upwards of 100 mW at 585 nm which excites the $6P_{3/2}$ atoms up to the $9D_{5/2}$ state. Via laser absorption it is estimated that there is a density of 4×10^9 cesium atoms/cm^3 excited to the $9D_{5/2}$ Rydberg state. Ions of helium and lithium passing through this region exchange charge resonantly with the $9D_{5/2}$ Cs, and neutralize into Rydberg states. From measurements at the Faraday cup (at 3 in Fig. 1) it is found that approximately 1% of the ion beam is neutralized by utilizing this charge-exchange technique. Thus the method allows us to produce a beam of neutral Rydberg states of helium or lithium (or any other atom or molecule) of 10 nA (6×10^{10}/s). Work is in progress to improve this already very successful technique to allow near 100% neutralization by increasing Cs density and laser powers. Approximately 10% of the neutral beam is found to exchange charge resonantly into the $n=10$ state. The use of resonant charge exchange proved to be a very effective method for creating large quantities for both helium and lithium Rydberg atoms for these measurements, and as such is a realization of a Rydberg target concept tested in earlier preliminary measurements [11].

The remaining (un-neutralized) ions are deflected out of the beam line (at 3 in Fig. 1) while the neutral atoms proceed into the first laser interaction region (at 4 in Fig. 1). Here a GTE Sylvania 950 CO_2 laser is used to drive a $10G$-to-$25H$ transition. The $^{13}C\,^{16}O_2$ laser is tuned to the $R\,10$ line at 10.849 μm and fine tuned by varying the angle of intersection between the laser and the atomic beam (thus varying the Doppler shift). The purpose of this laser transition is to depopulate the $10G$ state selectively.

The beam passes through a set of collimators (at 5 in Fig. 1) which along with a second set of collimators (at 8 in Fig. 1) places a 4-mrad limit on the spread of the atomic beam.

The atoms then enter a rf region where the transitions of interest are stimulated (at 6 in Fig. 1). The region is a 50-Ω rf transmission line, made out of copper waveguide (WR-430) as the outer conductor (4.30×2.15 in.^{2}) and a 1.125-in.-diameter copper cylinder as the inner conductor. The region was designed to have a 50-Ω characteristic impedance and to minimize excess capacitance near the ends where 50-Ω type-N rf connectors are used. The rf region is positioned parallel to the beamline and is a total of 49.8 cm long, giving an interaction time for the atoms traveling through it (at $\beta=0.001\,03$) of 1.61 μs. The beam which has a cross-sectional area of 0.25×0.25 in.^{2} passes through the center of the transmission line. The rf electric-field amplitude is constant to within 10% in this cross-sectional area. At both ends, 2×2 in.^{2} square holes allow the beam through and 2-in.-long copper shrouds limit fields entering or leaving the region. Before use, the rf region was tested using a voltage standing-wave ratio (VSWR) bridge and modified until it was found to have rf reflections of $|\Gamma|<0.02$ for the frequencies of interest. At both ends of the rf region, attenuators selected for small reflection coefficients ($|\Gamma|<0.015$) were placed in an effort to limit further rf reflections. The rf was provided by a 2022D Marconi signal generator externally amplitude modulated and computer controlled to scan through a set of frequencies of interest. The rf region drives the transitions from the $10H$ state to the previously depopulated $10G$ state.

The fact that this rf transition has been made is detected by a two-step process: excitation of the $10G$ atoms to $n=25$, followed by Stark ionization of the $n=25$ atoms. This is a very efficient method for detection of $n=10$ atoms, with a detection efficiency approaching 50%. In the second laser interaction region (at 7 in Fig. 1) the $10G$-to-$25H$ transition is again pumped, using the same CO_2 laser as was used in the fist interaction region. (A 50-50 beam splitter is used to give approximately 2 W to each region.)

The Stark-ionizing region is composed of two copper plates orthogonal to the beam with circular holes cut in them to allow the beam to pass through (see 9 in Fig. 1). It is designed to ionize all of the $n=25$ states but to leave the lower $n=10$ states unaffected and to do so utilizes an electric field of 3700 V/cm. The lower n states do not ionize and hit a shielded Faraday cup which is used primarily for beam diagnostics (see 11 of Fig. 1). The ions created in the Stark ionizer are deflected by a set of plates into a Galileo model 4720 channel electron multiplier (CEM) at 10 and 12 of Fig. 1.

The signal from the CEM is sent to a pair of EG&G 5105 lock-in amplifiers. One of the lock-in amplifiers is set to detect the signal synchronous with the am modulation frequency of the rf (100% am modulation done externally by a BK Precision 3010 function generator at 1400 Hz). The second is set to detect the signal synchronous with a 36-Hz chopper which chops the CO_2 laser and which allows 90% of its power through. Both signals are then sent to an analog-to-digital converter on a Stanford Research Labs SR850 lock-in amplifier which is then sent to the controlling computer via a GPIB interface, displayed, and stored for later analysis. The first signal is our main rf signal and shows the resonant transfer from $10H$ to $10G$ as the rf is tuned across the frequencies of interest. The second signal is used as a monitor, and indicates the efficiency of producing and resonantly neutralizing He or Li ions, and of CO_2 excitation, Stark ionization, and detection of the atoms of interest. This monitor signal is used to normalize the rf signal.

The process for observing the $10I$-to-$10H$ transitions exactly parallels the description of the $10H$-to-$10G$ transitions just described. The $10\,^3G_5-10\,^3H_6$ and

$10\,^3H_6-10\,^3I_7$ intervals in helium were also observed using the same technique. These intervals were measured as a check of systematic effects in the lithium measurements.

MEASUREMENTS

The data consist of several hundred scans of the $n=10$ resonances, with each scan consisting of approximately 50 data points taken at 50 discrete frequencies near the resonant features. The data points were taken in a symmetric fashion so as to reduce the effects of any signal fluctuations. Typical scans of lithium $10G$-$10H$ and $10H$-$10I$ transitions are shown in Fig. 2. The two-peaked structure in each of these scans results from the spin-orbit coupling for these states. The hyperfine structure is much smaller and is completely unresolved. The width of the resonances is limited by the interaction time of the atoms in the interaction region. Using 9 μW of rf power (just below the saturation power) causes most of the atoms to undergo transitions. Data are taken with the rf propagation both parallel and antiparallel to the direction of the beam's propagation and on a dozen separate days spanning a two-month period.

The expected line shape for these resonances is that of a two-level system interacting with a sinusoidal field for a time T:

$$S(\nu)=4CV^2\left[\frac{\sin(\pi bT)}{b}\right]^2, \tag{1}$$

where

$$b=[(2V)^2+(\nu-\nu_0)^2]^{1/2}$$

and

$$V=\frac{eE}{2h}\langle 10G_J|z|10H_{J+1}\rangle .$$

Here ν is the frequency at which the signal S is observed, ν_0 is the line center, E is the amplitude of the rf field, and C is the amplitude of the resonance. This line shape ignores the variation of the z matrix elements for individual m states—using instead of one matrix element which is an average over m states. Our modeling shows this approximation to have very little effect. Also ignored in Eq. (1) are the effects of the lifetimes of the states involved. Again this effect can be shown to be very small—a result which follows from the fact that the two states have similar lifetimes. Two other effects not included in Eq. (1) *are* expected to be important. The first is that the rf field does not turn on and off suddenly, but rather ramps up over about a 0.2 μs time as the atoms enter and leave the rf region. The second effect, which is just as important, is that while the atoms are inside the interaction region some atoms will transfer into $10G$, H, and I levels of interest due to radiative decay of higher-lying states as well as blackbody-induced radiative transfer from neighboring n levels. If such transfer occurs within the rf interaction region, the newly created $n=10$ atoms have a shorter time to interact with the rf, leading to a broadening of the rf resonance. Each of these effects could lead to broadening of up to 10%.

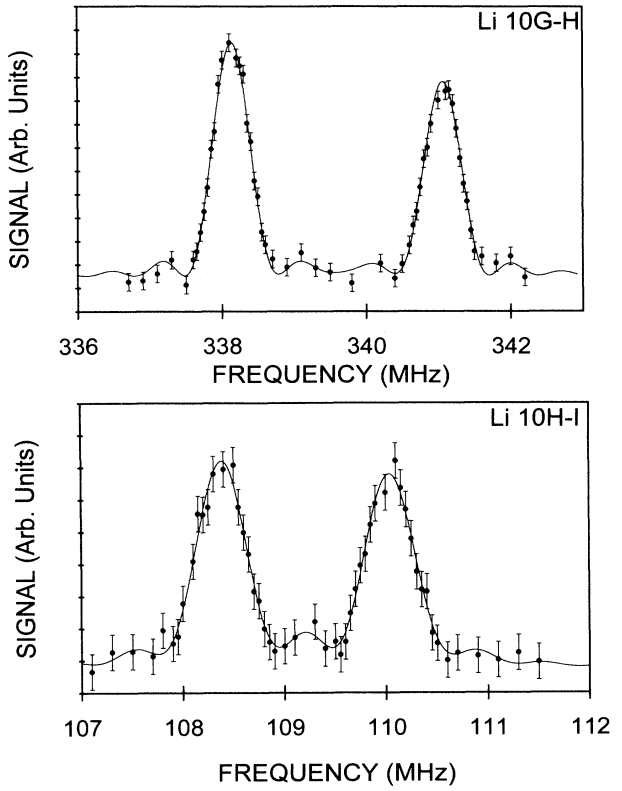

FIG. 2. Lithium $10G$-$10H$ and $10H$-$10I$ resonance data. Each data point in the plots represents 30 s of data collection. The peaks have been fitted to the line shape given by Eq. (1), and that best-fit curve is given by the solid line. Both plots represent data taken with the rf traveling parallel to the Rydberg beam.

To account for these broadening mechanisms, the parameter T was allowed to float (along with the parameters C and ν_0) in the least-squares fits of the data scans to the line shape of Eq. (1). As expected, the T's obtained from the fit were somewhat smaller than the actual 1.6 μs interaction time (by about 10%), indicating the presence of the broadening mechanisms mentioned above.

Because of these broadening mechanisms, Eq. (1) is not the entirely correct line shape for these resonances. For instance, the broadening due to blackbody-induced transitions from nearby states leads to a broadened line shape given by [6]

$$S(\nu)=(1-\alpha)4CV^2\left[\frac{\sin(\pi bT)}{b}\right]^2 e^{-\gamma T}+\frac{4CV^2\alpha}{Tb^2}\left[\frac{e^{-\gamma T}}{-2\gamma}-\frac{e^{-\gamma T}}{\gamma^2+4\pi^2b^2}\left[\frac{-\gamma}{2}\cos(2\pi bT)+\pi b\sin(2\pi bT)\right]+\frac{1}{2\gamma}+\frac{-\gamma/2}{\gamma^2+4\pi^2b^2}\right], \tag{2}$$

where

$$b=[(2V)^2+(\nu-\nu_0)^2]^{1/2}$$

and

$$\gamma=\frac{1}{2}\left[\frac{1}{\tau_i}+\frac{1}{\tau_f}\right],$$

with $(1-\alpha)$ being the fraction of the number of atoms which are present for the entire time T, τ_i and τ_f being the lifetimes of the initial and final states, and the other parameters identical to those defined for Eq. (1). The exact value of α depends on the populations of all of the nearby Rydberg states and since these are unknown we fit the data to Eq. (2) allowing α to float. The broadening mechanism due to the field ramping up on entering the rf cavity is modeled by the line shape given as follows:

$$S(\nu)=CV^2\left[\frac{2\sin(\pi bT)}{b}+\frac{\sin(\pi b_+T)}{b_+}+\frac{\sin[\pi b_-T]}{b_-}\right]^2, \tag{3}$$

where

$$b=\sqrt{(2V)^2+(\nu-\nu_0)^2},$$

$$b_\pm=\sqrt{(2V)^2+(\nu-\nu_0\pm\Delta)^2}.$$

Here $\Delta=1/T$ with all other symbols as previously defined in Eq. 1. This line shape is based on the electric field in the rf region being given by $E=E_0[\frac{1}{2}+\frac{1}{2}\cos(2\pi t/T)]$ where $-(T/2)<t<(T/2)$. This is a slower ramping than is actually expected in our region and thus will lead to an exaggerated effect on the line shape. The data were fitted to both of the above broadened line shapes as well as the shape given in Eq. (1). Here V and T were allowed to float while fitting. Further fits were done with either one or both of V and T kept constant. It was found that the peak centers were independent of the specific line shape used and independent of the parameters which were allowed to float. In all cases the centers that were obtained were in agreement to within a small fraction of the quoted error and thus we note that knowledge of the exact shape of the line is not necessary to obtain line centers to this accuracy. Data obtained from averaging many G-to-H scans are shown in Fig. 3 along with fitted lines for the three different line shapes. The data were also refitted allowing for a possible linear background $A+B\nu$ added to Eq. (1). Such fits returned linear constants (B) which were consistent with zero and again shifted the line centers much less than the final quoted error.

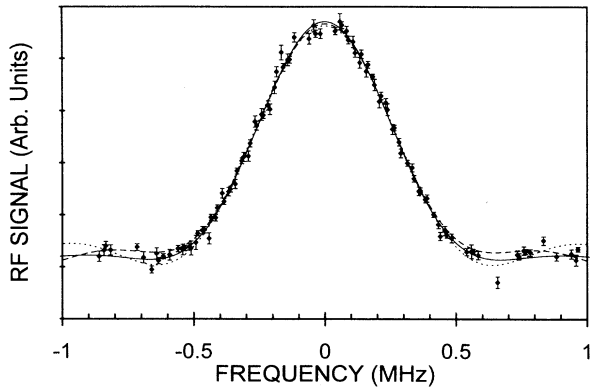

FIG. 3. Lithium $10G$-to-$10H$ shape. The data are an average of all lithium $10G$-to-$10H$ resonance scans. The dotted, dashed, and solid lines are least-squared fits of the data to Eqs. (1), (2), and (3), respectively. All three fits give the same line center to within much less than the statistically quoted uncertainties of Table I.

The final average of line centers obtained from least-squares fits of the resonance are given in columns 2 and 3 of Table I. The errors shown are statistical errors and also include the much smaller errors due to the fact that fits to different line shapes gave slightly different centers. The centers are in each case averages over several dozen scans taken in at least three separate runs on three separate days. No statistically significant variations were found when comparing data from different days. Columns 2 and 3, respectively, represent data taken with the rf propagating parallel and antiparallel to the direction of the atomic beam. Due to the Doppler shifts these are expected to be at

$$\nu_\pm=\nu_0\frac{1\pm\beta}{\sqrt{1-\beta^2}},$$

TABLE I. Measured lithium and helium intervals. The second and third columns list the line centers of the resonances obtained with the rf traveling parallel and antiparallel to the beam direction. The fourth column gives the geometric mean of these two columns. The fifth and sixth columns are the systematic effects due to rf reflections and Stark shifts. The last column gives the final corrected values of the peak centers. One standard deviation errors are given in parentheses and all values are in MHz.

	Center parallel	Center antiparallel	Geometric mean	rf reflection systematic	Stark-shift corrections	Final measured values
Li $10G_{9/2}$ to $10H_{11/2}$	338.1348(18)	338.8169(26)	338.4757(16)	0.0000(19)	0.0021(21)	338.4778(33)
Li $10G_{7/2}$ to $10H_{9/2}$	341.0600(24)	341.7415(32)	341.4006(20)	0.0000(19)	0.0021(21)	341.4027(35)
Li $10H_{11/2}$ to $10I_{13/2}$	108.3718(41)	108.5869(40)	108.4793(29)	0.0000(33)	0.0026(26)	108.4819(51)
Li $10H_{9/2}$to$10I_{11/2}$	110.0437(46)	110.2645(46)	110.1540(33)	0.0000(33)	0.0026(26)	110.1566(54)
He $10^3G_5$to 10^3H_6	491.4617(42)	492.4636(40)	491.9624(31)	0.0000(4)	[a]	491.9624(31)[a]
He 10^3H_6 to 10^3I_7	157.4669(24)	157.7868(24)	157.6268(20)	0.0000(4)	[a]	157.6268(20)[a]

[a]The values in helium are not corrected for dc Stark shifts since they are used to determine the size of the dc electric field present in the rf interaction region.

respectively, where ν_0 is the unshifted center. The geometric mean of these [i.e., $(\nu_+\nu_-)^{1/2}$] exactly equals ν_0 and is given in column 4 of Table I. To these centers, several systematic corrections must be applied. Only two effects are non-negligible and even these lead to corrections which are smaller than the statistical uncertainties.

The first effect is due to rf reflections. Because of reflections from the ends of the rf region, there is a small rf field which travels in the opposite direction and thus has the opposite Doppler shift when observed by the moving atoms. For our region with $|\Gamma|<0.02$ (along with attenuators with $|\Gamma|\cong 0.01$), the reflected wave had an amplitude which is reduced by a factor of at least 0.03 and thus a power reduced by more than a factor of 1000. This reflected wave distorts the line shape and thus shifts the resonances slightly. Fortunately, the reflections from the two ends (both from the ends of the rf region itself and from the attenuators at each end) are almost identical in amplitude and phase. To the extent that they are exactly equal, the effect exactly cancels when averaged over data taken with the rf propagating parallel and antiparallel to the beam propagation direction. Using a VSWR bridge and interference between various reflected waves, we determined that the reflections from the two ends of the region agree to within $|\Delta\Gamma|<0.010$. To account for possible differences in these reflections, we have modeled the effect using time-dependent perturbation theory and have included in column 5 of Table I a systematic uncertainty corresponding to the modeled effect due to $|\Delta\Gamma|=0.010$. Note that the two helium measurements are insensitive to reflection effects—a result which follows quite coincidentally from the two rf frequencies and the interaction time of the atoms in the field.

The two helium measurements were carried out in parallel with the lithium measurements to test for systematic effects—especially dc electric fields in the rf region which could lead to Stark shifts of the resonances. Great care was taken to make these dc fields small. The region was at the center of a set of large coils which reduced the rms magnetic field in the region to less than 15 mG. This reduced the $\vec{\beta}\times\vec{B}$ (motional) electric fields to less than 5 mV/cm. The region was constructed completely of copper to eliminate contact potentials between dissimilar metals. The region was carefully cleaned and also heated between runs to remove any dirt and oils from the surfaces, thus reducing surface charging.

To test for the presence of dc electric fields in the region, the two intervals in helium ($10\,^3G_5-10\,^3H_6$ and $10\,^3H_6-10\,^3I_7$) were measured and compared to previously measured values [6]. The current helium measurements are 0.9 ± 3.2 and 2.0 ± 2.0 kHz smaller than the most recent previous measurements [6] for the $10G$-to-H and the $10H$-to-I intervals, respectively. The level of agreement with the known values is used to set a limit on the size of a possible dc field in the rf region. Using Stark-shift rates for the $10G$-to-H and $10H$-to-I transitions in helium [12] of $-12(1)$, and $-15(1)$ MHz/(V/cm)^2 gives estimates of the electric field squared of 70 ± 260 and 130 ± 130 (mV/cm)^2, which indicates that E^2 is between 0 and 240 (mV/cm)^2 and thus E is between 0 and 15 mV/cm. The Stark-shift corrections shown in column 6 of Table I are obtained using Stark-shift rates for lithium [12] of $-17(1)$ and $-22(1)$ MHz/(V/cm)^2 for the $10G$-to-H and $10H$-to-I intervals, respectively. These Stark-shift corrections are then added with the rf reflection corrections to obtain a final peak center as shown in final column of Table I. Corrections due to ac Stark shifts, both those due to the rf field and those due to blackbody radiation [13], are smaller than 10% of the final quoted uncertainties and thus need not be included.

DISCUSSION OF RESULTS

The final column of Table I gives the four lithium intervals measured in the present work. The accuracies of 3–5 kHz are by far the most precise for any Rydberg lithium measurements. The separations between the pair of G-to-H resonances is due entirely to spin-orbit coupling (including Thomas precession) of the outer electron. Its value from Table I (considering only errors that affect the separations) is 2.9249 ± 0.0026 MHz. The similar separation between the H and I resonances is 1.6747 ± 0.0044 MHz. The simple hydrogenic expression

$$\Delta E_{\rm SO}=\frac{-\alpha^2 R}{n^3}\left[\frac{1}{j+\frac{1}{2}}\right] \tag{4}$$

for the spin-orbit shift from each state predicts the separations between the resonances to be 2.9198 and 1.6685 MHz, which show poor agreement with the measured values. If, however, the anomalous moment of the electron is properly included, Eq. (4) is multiplied by the factor $g-1\cong 1+\alpha/\pi$ and the predicted intervals are 2.9266 and 1.6723 MHz, in excellent agreement with our experimental values.

The positions of the lithium resonances are compared to the recent polarization-model predictions of Drachman and Bhatia [10] in Table II. Since the theoretical values of Drachman and Bhatia do not include the effect of spin, our measured lithium intervals are first corrected for spin-orbit contributions [using Eq. (2) multiplied by $g-1$] as shown in column 3 of Table II. Once corrected for spin effects, both the $10G_{7/2}$-$H_{9/2}$ and $10G_{9/2}$-$H_{11/2}$ intervals give experimental predictions for the spinless lithium $10G$-to-H interval. The two predictions are consistent with one another and give an average value (with proper propagation of errors which are common to both intervals) of 339.7186 ± 0.0031 MHz as shown in column 4. The similar pair of values are also consistent with each other for the H-to-I intervals and these average 109.2141 ± 0.0047 MHz as also shown in column 4. These two spinless values can then be compared directly to the values of Drachman and Bhatia as shown in column 5. For the $10G$-to-H interval, experiment and theory agree to within the 114-kHz uncertainty of the polarization-model predictions. For the $10H$-to-I interval, however, where the polarization-model predictions are more precise, there is a disagreement of seven standard deviations, with theory being larger than expected by 33 kHz. The most probable source of this discrepancy arises from relativistic corrections. In helium, the relativistic corrections to the dipole polarizability of He^+

TABLE II. Comparison to theory. The second column gives our measured values for the lithium intervals. The next column shows the expected spin-orbit contribution for these intervals. The fourth column gives the measured values corrected to remove the spin-orbit contributions. The two values thus obtained are averaged and listed in the row labeled $10G$ to $10H$. This and the similar $10H$-$10I$ value can be directly compared to recent polarization-model predictions listed in the Theory column. The final column gives the difference between experiment and theory. All values in the table are given in MHz, with one standard deviation error estimates given in parentheses.

	Experiment	Theoretical spin structure	Experiment without spin	Theory[a]	Experiment minus theory
$10G_{9/2}$ to $10H_{11/2}$	338.4778(33)	1.2416	339.7194(33)		
$10G_{7/2}$ to $10H_{9/2}$	341.4027(35)	−1.6850	339.7177(35)		
$10G$ to $10H$			339.7186(31)	339.80(11)	−0.08(11)
$10H_{11/2}$ to $10I_{13/2}$	108.4819(51)	0.7309	109.2128(51)		
$10H_{9/2}$ to $10I_{11/2}$	110.1566(54)	−0.9414	109.2152(54)		
$10H$ to $10I$			109.2140(47)	109.2466(11)	−0.0326(48)

[a]Reference [10].

contribute −34 kHz [14] to the $10H$-to-I interval. The relativistic correction to the Li^+ dipole polarizability has not yet been calculated and the present measurement indicates the need for its calculation, as well as calculation of other relativistic corrections to the structure. The retardation (Casimir) effect for these states has been estimated [15] to be −15 kHz for the $10H$-to-I interval. Therefore, when the relativistic corrections have been included, the present experiment will give a measurement of this effect to an accuracy of 25%.

CONCLUSION

Using a promising charge-exchange technique we have created large beams of Rydberg lithium atoms and used them for precise measurement of the lithium $10G$-to-$10H$ and $10H$-to-$10I$ intervals. The measurements show agreement with hydrogenic spin-orbit structure when the anomalous moment corrections are included. The primary purpose of the measurement, however, is to compare to recent polarization-model predictions of the structure which separates states of different L. Whereas the polarization model gives accurate predictions of the $10G$-H structure, the discrepancy in the $10H$-I interval indicates the need for the inclusion of relativistic effects in the theory. Further refinement of the Rydberg resonant charge-exchange method along with better control of systematic corrections could allow for much more precise measurements of these intervals as warranted by the increasing accuracy of theoretical predictions. The success of the resonant charge-exchange method will allow for a wide variety of Rydberg-atom measurements.

ACKNOWLEDGMENTS

This research was supported by the Natural Sciences and Engineering Research Council of Canada, to whom the authors extend their thanks. The authors would also like to thank Richard J. Drachman and A. K. Bhatia for communicating their theoretical results prior to publication.

[1] Richard J. Drachman, Phys. Rev. A **26**, 1228 (1982).

[2] S. L. Palfrey and S. R. Lundeen, Phys. Rev. Lett. **53**, 1141 (1984).

[3] C. K. Au, G. Feinberg, and J. Sucher, Phys. Rev. Lett. **53**, 1145 (1984); C. K. Au, Phys. Rev. A **31**, 1310 (1985); Richard J. Drachman *ibid.* **31**, 1253 (1985); **38**, 1659(E) (1988); **33**, 2780 (1986); James F. Babb and Larry Spruch, *ibid.* **36**, 456 (1987); G. Feinberg, C. K. Au, and J. Sucher, Ann. Phys. (N.Y.) **173**, 355 (1987); James F. Babb and Larry Spruch, Phys. Rev. A **38**, 13 (1988); C. K. Au, *ibid.* **39**, 2789 (1989); G. W. F. Drake, J. Phys. B **22**, L651 (1989); **23**, 1943(E) (1990); C. K. Au and M. A. Mesa, Phys. Rev. A **41**, 2848 (1990); G. W. F. Drake and Robin A. Swainson, *ibid.* **41**, 1243 (1990); G. W. F. Drake, Phys. Rev. Lett. **65**, 2769 (1990); C. K. Au, G. Feinberg, and J. Sucher, Phys. Rev. A **43**, 561 (1991); G. W. F. Drake, *ibid.* **45**, 70 (1992); **45**, 6933(E) (1992); G. W. F. Drake and Zong-Chao Yan, *ibid.* **46**, 2378 (1992); G. W. F. Drake and R. A. Swainson, *ibid.* **44**, 5448 (1991); S. P. Goldman and G. W. F. Drake, Phys. Rev. Lett. **68**, 1683 (1992); E. A. Hessels, Phys. Rev. A **46**, 5389 (1992); R. A. Swainson and G. W. F. Drake, Can. J. Phys. **70**, 187 (1992); Richard J. Drachman, Phys. Rev. A **47**, 694 (1993); G. W. F. Drake, Adv. At. Mol. Opt. Phys. **32**, 93 (1994).

[4] E. A. Hessels, W. G. Sturrus, S. R. Lundeen, and D. R. Cok, Phys. Rev. A **35**, 4489 (1987); **38**, 4574 (1988); E. A. Hessels, F. J. Deck, P. W. Arcuni, and S. R. Lundeen, *ibid.* **41**, 3663 (1990); Phys. Rev. Lett. **65**, 2765 (1990); **66**, 2544(E) (1991); Y. Kriescher, O. Hilt, and G. v. Oppen, Z. Phys. D **29**, 103 (1994).

[5] G. W. F. Drake, in *Long Range Casimir Forces: Theory and Recent Experiments in Atomic Systems,* edited by F. S. Levin, and D. Micha (Plenum, New York, 1993).

[6] E. A. Hessels, P. W. Arcuni, F. J. Deck, and S. R. Lundeen, Phys. Rev. A **46**, 2622 (1992).

[7] A. K. Bhatia and Richard J. Drachman, Phys. Rev. A **45**, 7752 (1992).

[8] D. K. McKenzie and G. W. F. Drake, Phys. Rev. A **44**, R6973 (1991); **48**, 4803(E) (1993).

[9] W. E. Cooke, J. F. Gallagher, R. M. Hill, and S. A. Edel-

stein, Phys. Rev. A **16**, 1141 (1977).
[10] Richard J. Drachman and A. K. Bhatia, following paper, Phys. Rev. A **51**, 2926 (1995).
[11] F. J. Deck, E. A. Hessels, and S. R. Lundeen, Phys. Rev. A **48**, 4400 (1993).
[12] The Stark-shift rates are obtained using hydrogenic matrix elements along with energy differences. The uncertainty in the rates results from the fact that each m level has a slightly different shift rate and the exact distribution of m levels present in our beam is not known.
[13] John W. Farley and William H. Wing, Phys. Rev. A **23**, 2397 (1981).
[14] Richard J. Drachman, Phys. Rev. A **31**, 1253 (1985).
[15] James F. Babb and Larry Spruch, Phys. Rev. A **40**, 2917 (1989).